POWER ELECTRONICS AND DRIVES
Vol. 2(37), No. 1, 2017 DOI: 10.5277/PED170110

POSITION TRACKING SYSTEMS FOR AC DRIVES EMPLOYING FORCED DYNAMICS CONTROL*

JAN VITTEK, LUKAS GOREL, VLADIMIR VAVRUS, LUBOS STRUHARNANSKY
University of Žilina, Univerzitna 1, 010 26 Žilina, Slovak Republic,
email address: jan.vittek@fel.uniza.sk

Abstract: Position tracking systems for AC drives offering high robustness to external load torques have been presented. A triple-loop cascade control structure was employed where the inner loop is a stator current control loop and the middle loop is a speed control loop based on the forced dynamic control and respecting vector control principles. Two alternative outer position control loop designs both of which respect prescribed dynamics and settling time of position have been developed. The former system prescribes also time constant of the speed control loop while the latter one respects time constant of speed control system developed independently. To enhance the tracking abilities of both control systems the dynamic lag pre-compensator has been included. Case studies of the both position control systems for time near-optimal control and energy near-optimal control have been presented. The tracking performances of the designed control systems were assessed based on comparisons of the experimental responses with the simulated responses of the ideal closed-loop system.

Keywords: *position control, AC drives, vector control, forced dynamics control, observer*

1. INTRODUCTION

The position control system for AC drive presented here is intended to operate in forced dynamics control (FDC) [1] respecting field oriented control (FOC) principles [2] and providing better robustness due to exploitation of load torque estimation from observer for the development of position control strategies.

The inner loop is a form of bang-bang control loop in which the stator currents are made to follow corresponding demands as closely as possible by switching the power electronic switching states to an appropriate value. The effect of this is similar to the hysteresis controller but the hysteresis element is unnecessary because the maximum power electronic switching frequency is automatically limited to $1/h$, where h is the achieved iteration interval of the micro-processor implementation. Thus, the motor is current fed and this eliminates the stator time constant from the problem of designing the middle and outer loop controllers.

*Manuscript received: May 15, 2017; accepted: July 4, 2017.

The middle loop controller controls the rotor speed using the FDC law, which causes the motor speed, ω_r, to follow the speed demand, ω'_{rd}, from the outer loop controller with a linear, first order dynamic lag having the time constant of T_ω. Since the middle loop controller is model based the closed-loop performance may be affected by errors in parameters estimates as well as in estimate of external load torque, Γ_L. The robustness of the speed control system against uncertain parameters and external load torques can be substantially improved by exploitation of a model reference adaptive control (MRAC) loop based on prescribed dynamics for this loop.

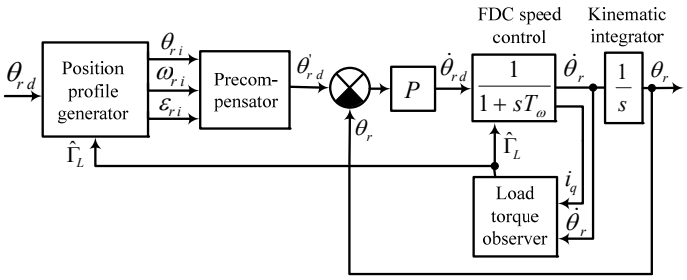

Fig. 1. Position control of AC drive with FDC of rotor speed

The purpose of the outer loop controller is to form prescribed time function of position response, $\theta_{ri}(t)$ together with corresponding state variables, acceleration, $\varepsilon_{ri}(t)$, and angular speed, $\omega_{ri}(t)$. The simulation results and preliminary experiments already obtained suggest that this control method for converters with higher switching frequencies could form the basis for a new generation of drives with improved performance. The control system has a cascade control structure, as shown in Fig. 1.

2. POSITION CONTROL SYSTEM DESIGN

As the position control system has nested control structure, the brief mathematical description of induction motor (IM), permanent magnet synchronous motor (PMSM) and speed control loop design precede design of the two alternative outer loop position controllers, both employing high gains to obtain the robustness.

2.1. MATHEMATIC DESCRIPTION OF AC DRIVES

Mathematical models of AC motors respecting FOC principles are described with differential equations in a matrix form. IM model consists of stator current vector, **I**, rotor flux vector, **Ψ**, rotor speed, ω_r and rotor position, θ_r, formulated in the coordinate system rotating in arbitrary speed, ω_k, is:

$$\dot{\mathbf{I}} = c_1\left[\mathbf{U} - a_1\mathbf{I} + c_2\mathbf{P}(\omega_r)\boldsymbol{\Psi}\right] + p\omega_k\mathbf{T}^{\mathrm{T}}\mathbf{I} \tag{1}$$

$$\dot{\boldsymbol{\Psi}} = c_4\mathbf{I} - \mathbf{P}(\omega_r)\boldsymbol{\Psi} + p\omega_k\mathbf{T}^{\mathrm{T}}\boldsymbol{\Psi} \tag{2}$$

where $\mathbf{I}^T = [\imath_d \ \imath_q]$ is the stator current, $\mathbf{U}^T = [u_d \ u_q]$ is the stator voltage, $\boldsymbol{\Psi}^T = [\Psi_D \ \Psi_Q]$ is the rotor magnetic flux vector. The constants are given as: $c_1 = L_r/(L_sL_r - L_m^2)$, $c_2 = L_m/L_r$, $c_3 = R_r/L_r = 1/T_r$, $c_4 = L_m/T_r$, $c_5 = 1.5\mathrm{p}L_m/L_r$ and $a_1 = R_s + R_r(L_m^2/L_r^2)$, where L_s, L_r and L_m are the stator and rotor inductances and their mutual inductance, respectively. R_s and R_r are the stator and rotor resistances, ω_r is the mechanical rotor speed, and ω_k is the arbitrary chosen angular speed valid for reference frame rotating at ω_k. Matrices $\mathbf{P}(\omega_r)$ and $\mathbf{T}$ are defined as:

$$\mathbf{P}(\omega_r) = \begin{bmatrix} c_3 & p\,\omega_r \\ -p\,\omega_r & c_3 \end{bmatrix} \text{ and } \mathbf{T} = \begin{bmatrix} 0 & -1 \\ 1 & 0 \end{bmatrix} \tag{3}$$

Similar way the state model of PMSM consisting of vectors: stator current, **I**, stator flux, **Ψ**, rotor speed, ω_r, and rotor position, θ_r, formulated in the rotor-fixed d_q coordinate system has the form:

$$\dot{\mathbf{I}} = \mathbf{P}(\omega_r, R_s)\mathbf{I} - \frac{p\omega_r}{L_q}\boldsymbol{\Psi}_{PM} + \mathbf{L}_R\mathbf{U} \tag{4}$$

where $\boldsymbol{\Psi}^T = [\Psi_d \ \Psi_q]$ is the stator magnetic flux in which $\Psi_d = L_d i_d + \Psi_{PM}$ and $\Psi_q = L_q i_q$, $\mathbf{I}^T = [\imath_d \ \imath_q]$ is the stator current, $\mathbf{U}^T = [u_d \ u_q]$ is the stator voltage, respectively. L_d, L_q are the stator inductances in direct and quadratic axis and R_s is the stator resistance. Matrices $\mathbf{P}(\omega_r, R_s)$, $\boldsymbol{\Psi}_{PM}$ and $\mathbf{L}_R$ have form:

$$\mathbf{P}(\omega_r, R_s) = \begin{bmatrix} -\dfrac{R_s}{L_d} & \dfrac{p\omega_r L_q}{L_d} \\ -\dfrac{p\omega_r L_d}{L_q} & -\dfrac{R_s}{L_q} \end{bmatrix}, \ \boldsymbol{\Psi}_{PM} = \begin{bmatrix} 0 \\ \Psi_{PM} \end{bmatrix} \text{ and } \mathbf{L}_R = \begin{bmatrix} \dfrac{1}{L_d} & 0 \\ 0 & \dfrac{1}{L_q} \end{bmatrix} \tag{5}$$

The equations for rotor speed and position are common and differ in constant, c, only. Both differential equations are as follows:

$$\dot{\omega}_r = \frac{1}{J}\left(\Gamma_{el} - \Gamma_L\right) = \frac{1}{J}\left(c\boldsymbol{\Psi}^T\mathbf{T}^T\mathbf{I} - \Gamma_L\right) \tag{6}$$

$$\dot{\theta}_r = \omega_r \tag{7}$$

where Γ_{el} is the torque developed by the motor, J is moment of inertia related to motor shaft and p is the number of pole pairs. Constant, c, is given as $c = c_5 = 3pL_m/2L_r$ for IM and c = $3p/2$ for SMPM, respectively.

2.2. FORCED DYNAMICS SPEED CONTROL LOOP DESIGN

A common feature of designed control systems is a speed control loop of both types motors based on FDC while satisfying the FOC control conditions [3]. Rotor speed obeys (6) and the differential equation describing the closed loop dynamics have therefore a linear first order dynamics (8), where T_ω is the prescribed time constant and $\dot{\theta}_{rd}$ is the demanded rotor speed:

$$\ddot{\theta}_r = \frac{1}{T_\omega}\left(\dot{\theta}_{rd} - \dot{\theta}_r\right) \tag{8}$$

For the derivative of the rotor speed of both motors, the PMSM and IM is then valid:

$$\dot{\omega}_r = \frac{1}{J_r}\left(c\,\mathbf{\Psi}^T\mathbf{T}^T\mathbf{I} - \Gamma_L\right) = \begin{cases} \dfrac{1}{J_r}\left[c\left(\Psi_d i_q - \Psi_q i_d\right) - \Gamma_L\right] & \text{for the PMSM} \\ \dfrac{1}{J_r}\left[c\left(\Psi_D i_q - \Psi_Q i_d\right) - \Gamma_L\right] & \text{for the IM} \end{cases} \tag{9}$$

For the PMSM, Ψ_d and Ψ_q are the stator fluxes components, and $c = 3p/2$. For the IM, Ψ_D and Ψ_Q are the rotor fluxes components and $c = c_5$. Using a switched power electronic control law, the stator current components are made to follow their demands, $i_{d\mathrm{dem}}$ and $i_{q\mathrm{dem}}$, with negligible dynamic lag. Hence it is assumed that $i_d = i_{d\mathrm{dem}}$ and $i_q = i_{q\mathrm{dem}}$ which enables the stator current equations to be eliminated from the plant model for the control system design. This way for speed control, $i_{d\mathrm{dem}}$ and $i_{q\mathrm{dem}}$ are regarded as control variables. For FOC of PMSM up to the nominal speed $i_d = i_{d\mathrm{dem}} = 0$, and for rotor flux FOC of IM $\Psi_Q = 0$, so the terms, $\Psi_q i_d$ and $\Psi_Q i_d$ on the RHS of (9) vanish. Equating the RHS of (8) and (9) then yields the same speed control algorithm for both types of motors:

$$i_{d\,dem} = \begin{cases} 0 \text{ for the PMSM drive} \\ \text{const} \neq 0 \text{ for the IM drive} \end{cases} \quad \text{and} \quad i_{q\,dem} = \frac{1}{\Psi}\left\{\frac{1}{c}\left[\frac{J_r}{T_\omega}\left(\dot{\theta}_{r\,d} - \dot{\theta}_r\right)\right] + \Gamma_L\right\} \tag{10}$$

where $\Psi = \Psi_d$ for the PMSM drive and $\Psi = \Psi_D$ for the IM drive. A load torque observer can be used to estimate the net load torque, Γ_L, on the motor shaft [4].

2.3. FORCED DYNAMICS POSITION CONTROL LOOP DESIGN

For verification of control strategies requiring precise position tracking the two control structures consisting of position profile generator completed with a zero dynamic lag pre-compensator and FDC based position control loop are developed further.

The FDC system for speed control of the AC motors is already robust, because it produces a nominal closed-loop transfer function (8) that is independent of the load torque and motor moment of inertia [5]. Plant for position control is formed by FDC speed control loop replaced by its ideal transfer function (*the first order lag*) and completed with kinematic integrator, as it is shown in Fig. 2.

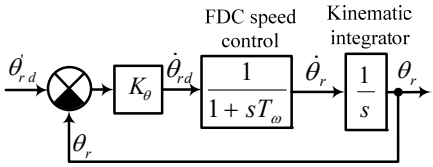

Fig. 2. Block diagram for position tracking control

Big advantage of FDC is that this control loop is of the second order and gain, K_θ and time constant, T_ω are variable parameters. Closed-loop transfer function is:

$$\frac{\theta_r(s)}{\theta_{rd}(s)} = \frac{\frac{K_\theta}{T_\omega}}{s^2 + \frac{s}{T_\omega} + \frac{K_\theta}{T_\omega}} \tag{11}$$

Parameters of position control loop may be designed by pole assignment using Dodds's settling time formula [6]:

$$\frac{\theta_r(s)}{\theta'_{rd}(s)} = \left[\frac{1}{1 + s\frac{T_{s\theta}}{1.5(1+n)}}\right]^n\Bigg|_{n=2} = \frac{\frac{81}{4T_{s\theta}^2}}{s^2 + \frac{9}{T_{s\theta}}s + \frac{81}{4T_{s\theta}^2}} \tag{12}$$

in which $T_{s\theta}$ is prescribed settling time of position control system. Following adjustment of these parameters results from comparison (11) and (12):

$$T_\omega = \frac{T_{s\theta}}{9} \text{ and } K_\theta = \frac{9}{4T_{s\theta}} \tag{13}$$

For position control system having already tuned FDC speed control loop with chosen time constant, T_ω, following approach enables to adjust parameters of the position control system. If the prescribed second order response (12) is converted into time domain yields for rotor position the second order closed loop differential equation:

$$\ddot{\theta}_r = \frac{81}{4T_{s\theta}^2}\left(\theta_{rd}^{'} - \theta_r\right) - \frac{9}{T_{s\theta}}\dot{\theta}_r \tag{14}$$

FDC law for rotor angle is then obtained by substituting (8) for LHS of (14) and solving this equation for the input variable, which is rotor speed demand, $\dot{\theta}_{rd}$:

$$\dot{\theta}_{rd} = \left(1 - \frac{9T_\omega}{T_{s\theta}}\right)\dot{\theta}_r + \frac{81T_\omega}{4T_{s\theta}^2}\left(\theta_{rd}^{'} - \theta_r\right) \tag{15}$$

Block diagram corresponding to derived control algorithm (15) is shown in Fig. 3.

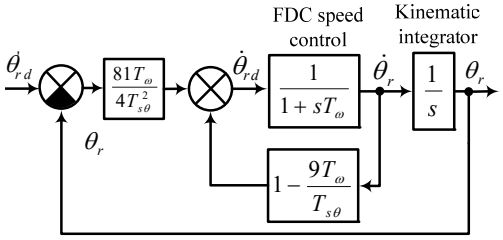

Fig. 3. Block diagram for position tracking control with respect of designed speed control loop

2.4. PRECOMPENSATOR AND LOAD TORQUE OBSERVER DESIGN

Closed loop dynamic of both position controllers is prescribed by (12), therefore the dynamic lag pre-compensator can be designed as the inverse transfer function as follows:

$$F_{PC}(s) = \frac{\theta_{rd}(s)}{\theta_r(s)} = s^2\frac{4T_s^2}{81} + s\frac{4T_s}{9} + 1 \tag{16}$$

2.5. LOAD TORRQUE OBSERVER DESIGN

The load torque estimate required by FDC speed control loop and useful also for generation of position profiles is provided by a standard observer having a similar structure to a Kalman filter, a direct measurement of this variable being assumed to be unavailable. The real time model of this observer is based on motor torque equation (9) and has form:

$$
\begin{aligned}
e_\omega &= \omega_r - \hat{\omega}_r \\
\dot{\hat{\omega}}_r &= \frac{1}{J}\left(c\Psi i_q - \hat{\Gamma}_L \right) + k_\omega e_\omega \\
\dot{\hat{\Gamma}}_L &= k_\Gamma e_\omega
\end{aligned}
\tag{17}
$$

This is a conventional second order linear observer with a correction loop characteristic polynomial which may be chosen via the gains, k_ω and k_Γ, as:

$$
k_\omega = \frac{9}{T_{so}} \text{ and } k_\Gamma = \frac{81J}{4T_{so}^2} \tag{18}
$$

where T_{so} is the observer prescribed settling time designed to yield the desired balance of filtering between the noise from the measurements of i_d and i_q and the noise from the angular velocity measurement [7].

3. TRACKING PERFORMANCES VERIFICATION

Two control strategies requiring precise position tracking were chosen for investigation of tracking performances of previously designed position control systems. The first strategy presents time near-optimal control exploiting full torque capabilities of the drive with PMSM while the second introduces energy near-optimal control based on symmetrical trapezoidal speed profile applied to IM.

3.1. TIME NEAR-OPTIMAL CONTROL OF AC DRIVES

The performance of many industrial electric drives employed in position control systems could be improved by minimizing the response time to step changes in the reference input. In general, time optimal control is a bang-bang control in which the control variable switches between its saturation limits.

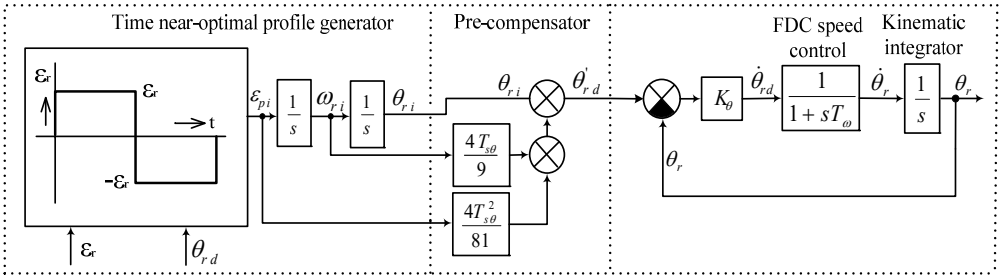

Fig. 4. Overall control system for time near-optimal position control

Due to the fact that the mathematical expression for the time-optimal switching boundary in the state space needed for higher order plant is rather complicated, a reduced second order model might be used to derive a closed-loop time optimal controller [8]. A structure consisting of a time near-optimal profile generator, pre-compensator and FDC position control loop shown in Fig. 4 is used for implementation.

The load torque, Γ_L, is assumed to be constant and the demanded rotor angle, θ_{rd} is constant. The time optimal control of such a plant has one switching during the rest to rest position maneuver leading to the desired state. The time optimal switching boundary then consists of the two parabolic segments coincident with the two trajectories leading directly to the origin of the error phase plane for $\Gamma_{el} = +\Gamma_{\max}$ and $\Gamma_{el} = -\Gamma_{\max}$. Corresponding time optimal control law can be in this case written as:

$$\Gamma_{el} = -\Gamma_{\max} \operatorname{sign}\left(S\right) \tag{19}$$

and switching boundary, S, has the form:

$$S = \theta_r - \theta_{r\,d} + \frac{1}{2\varepsilon_r}\,\omega_r \left|\omega_r\right| \tag{20}$$

where θ_{rd} is demanded position set-point, θ_r, is actual position and ω_r is rotor speed. Rotor acceleration is a function of the rotor speed, ω_r, as:

$$\varepsilon_r = \begin{cases} \dfrac{J_m}{2\left(\Gamma_{\max} + \Gamma_L\right)} & \text{for} \quad \omega_r < 0 \\ \dfrac{-J_m}{2\left(\Gamma_{\max} - \Gamma_L\right)} & \text{for} \quad \omega_r > 0 \end{cases} \tag{21}$$

Due to definition of switching boundary by (20) control law will suffer from control chatter about the phase-plane origin.

The control chatter can be eliminated by replacing the switching boundary by a boundary layer which is defined as:

$$\Gamma_{el} = \begin{cases} -\Gamma_{\max} K_b S & \text{for } K_b \left|S\right| < 1 \\ -\Gamma_{\max} \operatorname{sign}\left(S\right) & \text{for } K_b \left|S\right| > 1 \end{cases} \tag{22}$$

in which K_b should be set to longest possible value as limited by iteration interval, h. Due to zero damping, this modification results in an oscillatory response with a natural frequency $\omega_n = \sqrt{K_b}$. The damping is ensured by introducing a linear term, $T_d\omega_r$ to switching function which then becomes:

$$S = \theta_r - \theta_{rd} + T_d \omega_r + \frac{1}{2\varepsilon_r} \omega_r \left| \omega_r \right| \tag{23}$$

The value of T_d should be set to the smaller possible value as it allows iteration interval, h. This way defined switching function in control law maintains a non-oscillatory response of the control system.

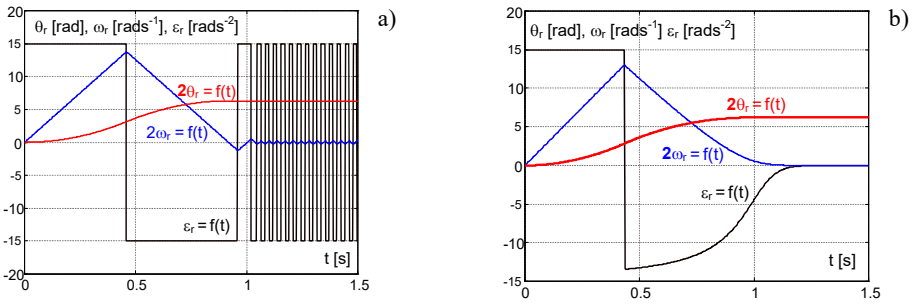

Fig. 5. The effect of switching boundary design

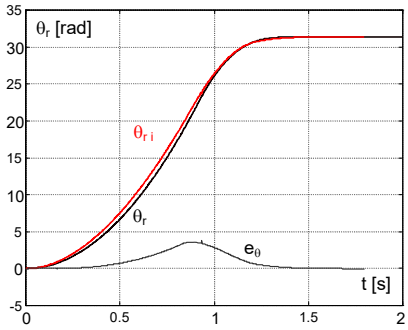

a) plant and model position responses

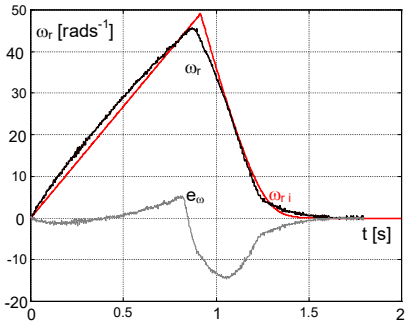

b) plant and model angular speed responses

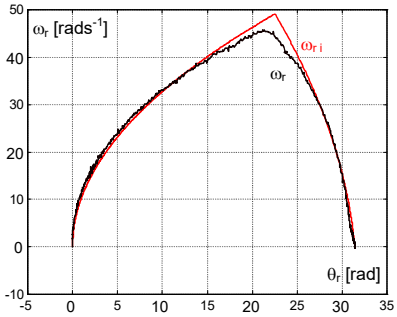

c) plant and model speed in function of position

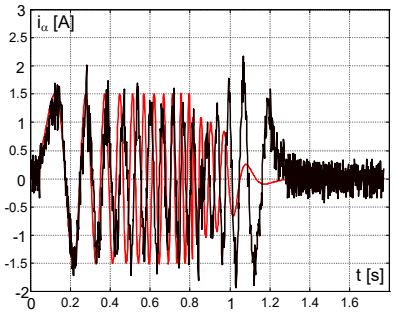

d) time dependence of plant and model stator current

Fig. 6. Model and real plant responses to NTO control

The effect of switching boundary design is shown in Fig. 5 for an idle running motor with $\Gamma_{\max} = 15$ N·m, $\theta_{rd} = 3.14$ rad and $J_r = 1$ kg·m^2. Figure 5a shows resulting rotor acceleration, speed and position corresponding to the switching boundary given by (20) including control chatter. The same state-variable are shown for switching boundary given by (23). In this case, the time of control is longer due to the damping term, therefore control is called near-time optimal (NTO).

The experiments with NTO control are shown in Fig. 6 for prescribed variables by time near-optimal profiles generator and real drive's motor responses. PMSM parameters used for experiments are listed in the Appendix. The demanded position was $\theta_{rd} = 31.4$ rad, achieved sampling frequency was 10 kHz and motor was loaded with a nominal torque. Figure 6a shows time functions of rotor position of the NTO model, $\theta_{ri}(t)$ and real rotor position $\theta_r(t)$ including differences between them. Figure 6b shows the prescribed rotor speed by the generator, $\omega_{ri}(t)$ and a real rotor speed, $\omega_r(t)$ including differences between them in function of time. Mutual dependence of model and rotor speed in function of their positions are shown in Fig. 6c, and Fig. 6d shows time dependences of the modelled and real phase currents.

The presented experimental results for NTO position control of electric drives employing PMSM confirm possibility to force the drive through time near-optimal model to tract prescribed state-variables and achieve demanded position. The significant, though not very large, departure from the ideal performance are mainly due to the non-zero iteration interval, differences in real and estimated load torque, and errors in parameter estimates.

3.2. NEAR-ENERGY OPTIMAL CONTROL OF AC DRIVES

Energy saving position control strategy for AC drives presented further minimizes electrical as well as mechanical losses consisting of constant, A, viscous, B, and quadratic, C, friction components. Strategy exploits a symmetrical trapezoidal speed profile, which respects prescribed maneuver time to reach demanded reference set-point.

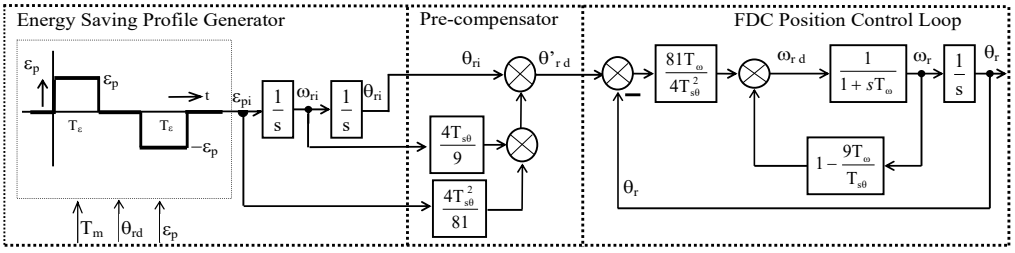

Fig. 7. Overall control system for energy near-optimal position control

An overall control system shown in Fig. 7 is model based and requires precise tracking of state variables (rotor acceleration, ε_{ri}, speed, ω_{ri} and position, θ_{ri}) generated in the energy saving profile generator.

Assuming symmetrical trapezoidal speed profile for rest to rest position maneuver, the time functions of stator current torque components covering the energy expenditures are shown in Fig. 8.

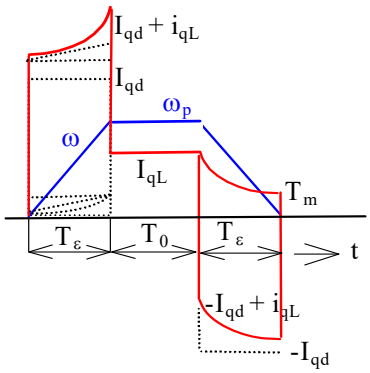

Fig. 8. Stator current torque components
for individual time-intervals of energy near-optimal control

Description of current torque components for three subsequent intervals is as follows:

$$i_q(t) = i_{q1}(t) + i_{q2}(t) + i_{q3}(t) \tag{24}$$

$$i_{q1}(t) = I_{qd} + i_{qL}(t),\ \ i_{q2}(t) = I_{qL},\ \ i_{q3}(t) = -I_{qd} + i_{qL}(t) \tag{25}$$

where currents I_{qd} and I_{qL} are constant while current i_{qL} is time varying during acceleration and deceleration period due to speed dependence of viscous and quadratic friction.

Total drive's energy allowing optimization, W_T is calculated from:

$$W_T = \frac{3}{2}\int_0^{T_m} R_s i_q^2 dt + \int_0^{T_m} \left(A + B\omega + C\omega^2\right)\omega dt \tag{26}$$

and results in:

$$W_T = \frac{\theta_{rd}^2}{\left(T_m - T_\varepsilon\right)^2}\left[\frac{k_1}{T_\varepsilon} + \frac{3R_s A^2}{2c\Psi^2}T_m + k_2\left(T_m - \frac{4}{3}T_\varepsilon\right) + k_3\frac{\theta_{rd}^2}{\left(T_m - T_\varepsilon\right)^2}\left(T_m - \frac{8}{5}T_\varepsilon\right)\right.$$
$$\left. + k_4\frac{\theta_{rd}}{\left(T_m - T_\varepsilon\right)}\left(T_m - \frac{4}{3}T_\varepsilon\right) + k_5\frac{\theta_{rd}}{\left(T_m - T_\varepsilon\right)}\left(T_m - \frac{3}{2}T_\varepsilon\right) + A\theta_{rd}\right] \tag{27}$$

in which the constants are defined as:

$$k_1 = 3R_s \frac{J_r^2}{c\Psi^2},\ k_2 = \frac{3}{2} R_s \frac{B^2}{c\Psi^2} + B,\ k_3 = \frac{3}{2} R_s \frac{C^2}{c\Psi^2}$$

$$k_4 = 3R_s \frac{AC}{c\Psi^2},\ k_5 = 3R_s \frac{BC}{c\Psi^2} + C,\ k_s = k_2 + k_4$$

To find minimum of (27), and to determine time of acceleration and deceleration, T_ε the derivative, dW_T/dT_ε is set to zero resulting in:

$$-\frac{4}{3}k_s T_\varepsilon^5 + \left(\frac{10}{3}k_s T_m + 3k_5\theta_{rd}\right)T_\varepsilon^4 + \left(3k_1 - \frac{2}{3}k_s T_m^2 - \frac{9}{2}k_5\theta_{rd}T_m - \frac{24}{5}k_3\theta_{rd}^2\right)T_\varepsilon^3$$
$$+\left(-7k_1 + \frac{2}{3}k_s T_m^3 + \frac{3}{2}k_5\theta_{rd}T_m^2 + \frac{12}{5}k_3\theta_{rd}^2 T_m\right)T_\varepsilon^2 + 5k_1 T_m^2 T_\varepsilon - k_1 T_m^3 = 0 \qquad (28)$$

which is the fifth order algebraic equation. To determine required acceleration time, T_ε, the zeros of (25) have to be found and a Newton formula having quadratic convergence is used for.

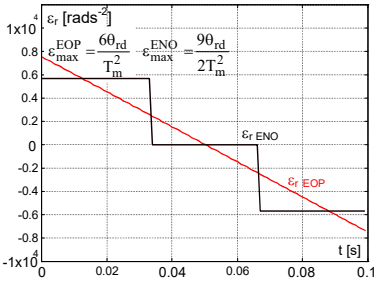

a) acceleration profiles

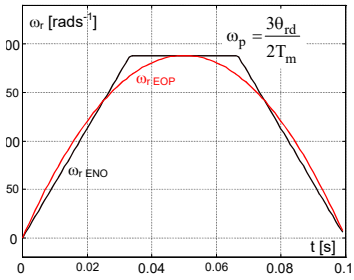

b) angular speed profiles

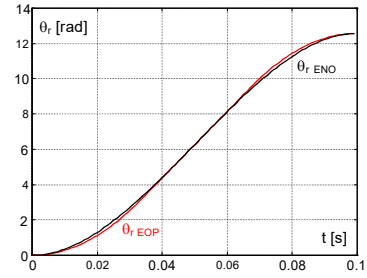

c) position profiles

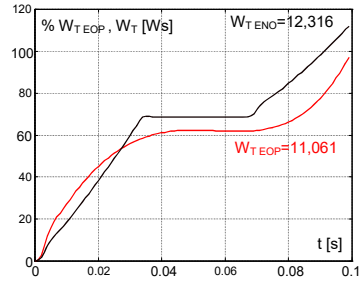

d) energy consumption

Fig. 9. Comparison of energy optimal and near-optimal control strategies

Comparison of the state variables for energy optimal (EOP) and energy near optimal control (ENO) together with energy consumption for the lumped moment of inertia $J = 1$ kg·m^2 is shown in Fig. 9. Figure 9a shows required acceleration for the prescribed maneuver time, $T_m = 0.1$ s and for constant load torque, $\Gamma_L = 1$ N·m. As can be seen from Fig. 9b, the symmetrical trapezoidal rotor speed profile of ENO has the same magnitude of angular speed as EOP and trapezoidal speed profile well fits the speed profile of EOP. Corresponding position time profiles are shown in Fig. 9c. Energy consumption of both profiles is shown in Fig. 9d from which can be observed that consumption of ENO control is only by 11.35% higher than that of EOP one. More details on energy optimal and near optimal control can be found in [9].

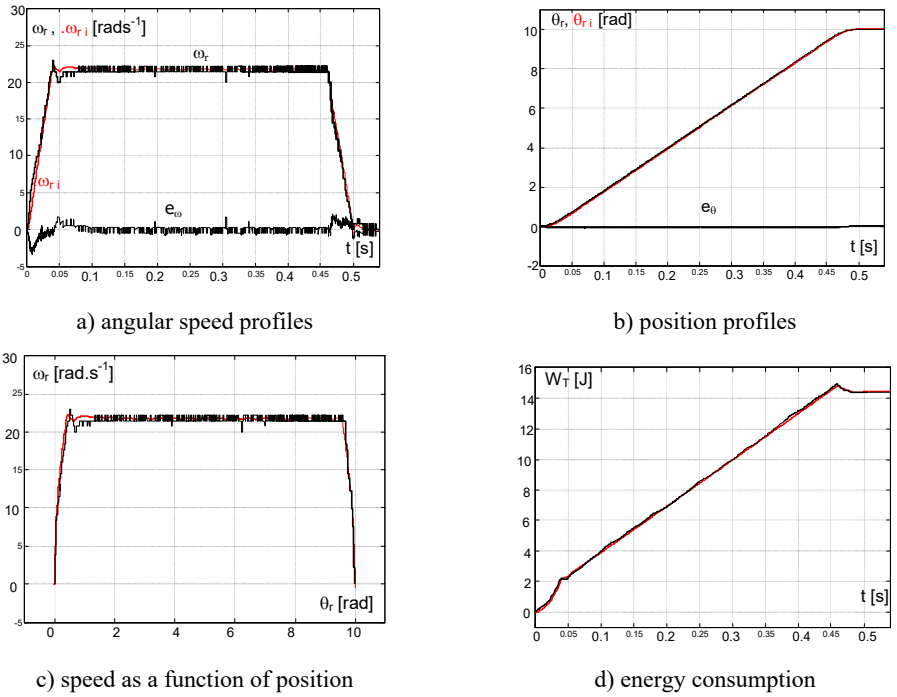

a) angular speed profiles

b) position profiles

c) speed as a function of position

d) energy consumption

Fig. 10. Comparison of energy optimal and near-optimal control strategies

The results of experiments with ENO control are shown in Fig. 10 for state variables generated by energy saving profile generator and real rotor responses. For this energy saving, control strategy IM parameters (cf. Appendix) was used in experiments. IM was loaded with PM synchronous generator supplying constant resistive load. The prescribed maneuver time, $T_m = 0.5$ s, demanded position θ_{rd} was 10 rad, and achieved sampling frequency in experiments was 10 kHz. The parameters of load components were identified off-line as a constant torque component, $A = 0.166$ N·m, and a viscous component proportional to the rotor speed, $B = 0.0531$ N·m·s.

If there are speed limitations on the track or limitation of drives maximum speed, such travel time for travelling this distance with prescribed speed should subtracted from prescribed manoeuvre time and a new movement in a new travel time should be derived by the energy saving profile generator. In this case, it is necessary also to check limit of allowed drive's acceleration. If limits of acceleration are exceeded, a new prescribed manoeuvre time is suggested.

Figure 10a shows the prescribed speed profile by the NTO model, $\omega_{ri}(t)$, and a real rotor speed, $\omega_r(t)$, in function of time as well as the difference between them. Figure 10b shows time dependences of rotor position of the NTO model, $\theta_{ri}(t)$, and a real rotor position, $\theta_r(t)$, including tracking error between them. Mutual functions of generated and real rotor speed in function of corresponding positions are shown in Fig. 10c. Figure 10d shows time dependences of total energy consumption, W_T, of the modelled drive with IM and a computed one as time integral of input power:

$$W_T = \frac{3}{2}\int_0^{T_m} \left(u_q i_q + u_d i_d \right) dt \tag{29}$$

and total energy consumption of real drive measured by vector wattmeter. As can be seen from this figure, good agreement of computed and measured energy consumption was achieved.

The presented experimental results for ENO position control of electric drives employing IM confirm possibility to force the drive to follow prescribed state-variables by energy saving profile generator and reach demanded position in prescribed maneuver time.

4. CONCLUSIONS AND RECOMMENDATIONS

Advantage of FDC of AC drives speed with linear first order dynamics has been exploited for the design of the two modified position control systems based on the second order dynamics. Prescribed arbitrary second order position response allows implementation of dynamic lag pre-compensator, which substantially improves control performance of the designed systems.

Implementation of FOC drives together with FDC laws, which yields known linear closed loop dynamics together with a dynamic lag eliminating pre-compensator enabled to follow accurately easily pre-computed near time optimal and near energy optimal reference input functions, thereby forcing the control systems to react with a near-optimal behavior.

Presented case studies for time near-optimal and energy near-optimal control of the drives employing AC motors confirmed good tracking abilities of the designed position control systems not only in simulations but also in laboratory experiments. The position

control systems, as developed to date, would be suited very well to applications requiring position control with a moderate accuracy.

APPENDIX

Parameters of PMSM equivalent circuit: rated power, $P_n = 375$ W, at $\omega_n = 314.16$ rad/s, number of pole pairs, $p = 3$, stator resistance, $R_s = 3.65\ \Omega$, direct and quadrature axes inductances, $L_d = L_q = 50$ mH; permanent magnet linkage flux, $\Psi_{PM} = 0.312$ V·s, the lumped moment of inertia was $J = 0.0032$ kg·m^2 and applied load torque, $\Gamma_L = 1$ N·m was developed by IM operating in plugging mode.

Parameters of IM equivalent circuit: rated power, $P_n = 1.5$ kW, at a speed of $n_n = 1420$ rpm; rated current, $I_n = 2.4/4.2$ A, Y/Δ, terminal voltage, $U = 400/230$, Y/Δ. Stator, rotor resistances, $R_s = 5.155\ \Omega$, $R_R = 4.426\ \Omega$; stator, rotor inductances, $L_S = L_R = 0.291$ H, mutual inductance, $L_M = 0{,}271$ H; moment of inertia, $J = 0.0035$ kg·m^2.

REFERENCES

[1] DODDS S.J., *Feedback Control. Linear, Non-linear and Robust Techniques and Design with Industrial Applications*, Springer, London 2015, 481–550.

[2] LEONHARD W., *Control of Electrical Drives*, Springer-Verlag, Berlin 1997, 229–285.

[3] BRANDSTETTER P., KRECEK T., *Speed and current control of permanent magnet synchronous motor using IMC controllers*, Adv. El. Comp. Eng., 2012, 12(4), 3–10.

[4] VITTEK J., DODDS S.J., *Forced Dynamics Control of Electric Drives*, EDIS Publishing Centre of Zilina University, Slovakia, 2003, http://www.kves.uniza.sk/?menu = proj&page = Elearn

[5] DODDS S.J., VITTEK J., UTKIN A., *Sensorless induction motor drive with independent speed and rotor magnetic flux control. Part I. Theoretical background*, *Part II. Simulation and real-time implementation*, J. El. Eng., 1998, 49(7–10), 186–193, 232–239.

[6] DODDS S.J., *Settling time formulae for the design of control systems with linear closed loop dynamics*, International Conference AC&T, University of East London, UK, 2007.

[7] ORLOWSKA-KOWALSKA T., *Application of extended luenberger observer for flux and rotor time-constant estimation in induction motor drives*, Control Theory Appl., IEE Proc. D, 1989, 136(6), 324–330.

[8] RYAN E.P., *Optimal Relay and Saturating Control System Synthesis*, P. Peregrinus on behalf of the Institution of Electrical Engineers, Stevenage, UK, 1982, 79–97.

[9] VITTEK J., BUTKO P., FTOREK B., MAKYS P., GOREL L., *Energy near-optimal control strategies for industrial and traction drives with AC motors*, Math. Probl. Eng., 1987, 687–704, https://doi.org/10.1155/2017/1857186

[10] FEDOR P., PERDUKOVA D., *Energy optimization of a dynamic system controller*, International Joint Conference on Advances in Intelligent Systems and Computing AISC, Bangalore, India, 2013, 189, 361–369.

[11] ROZANOV Y., RYVKIN S., CHAPLYGIN E., VORONIN P., *Power Electronics. Basics, Operating Principles, Design, Formulas and Applications*, CRC Press, London 2016, 430–449.